

# RSC Advances



This is an *Accepted Manuscript*, which has been through the Royal Society of Chemistry peer review process and has been accepted for publication.

*Accepted Manuscripts* are published online shortly after acceptance, before technical editing, formatting and proof reading. Using this free service, authors can make their results available to the community, in citable form, before we publish the edited article. This *Accepted Manuscript* will be replaced by the edited, formatted and paginated article as soon as this is available.

You can find more information about *Accepted Manuscripts* in the [Information for Authors](#).

Please note that technical editing may introduce minor changes to the text and/or graphics, which may alter content. The journal's standard [Terms & Conditions](#) and the [Ethical guidelines](#) still apply. In no event shall the Royal Society of Chemistry be held responsible for any errors or omissions in this *Accepted Manuscript* or any consequences arising from the use of any information it contains.



## The $\text{Li}_4(\text{NH}_2)_3\text{Cl}$ amide-chloride: new synthesis route, hydrogen storage kinetic and thermodynamic properties†

N. S. Gamba,<sup>ab\*</sup> P. Arneodo Larochette<sup>abc</sup> and F. C. Gennari<sup>abc</sup>

Received 00th January 20xx,  
Accepted 00th January 20xx

DOI: 10.1039/x0xx00000x

www.rsc.org/

Amide-halide compounds were identified as possible promoters of the dehydrogenation kinetics of the Li-N-H system. However, reversible hydrogen storage capacities and sorption kinetics of  $\text{Li}_4(\text{NH}_2)_3\text{Cl}$  and  $\text{Li}_3\text{Mg}_{0.5}(\text{NH}_2)_3\text{Cl}$  were not reported yet. In the present work,  $\text{Li}_4(\text{NH}_2)_3\text{Cl}$  was synthesized by a new synthesis route that involves the pre-milling of the  $\text{LiNH}_2$ - $\text{LiCl}$  mixture. Attempts to synthesize  $\text{Li}_3\text{Mg}_{0.5}(\text{NH}_2)_3\text{Cl}$  by applying similar synthesis procedure from  $\text{LiNH}_2$  and  $0.5\text{MgCl}_2$  were unsuccessful; instead, a mixture of  $\text{Li}_4(\text{NH}_2)_3\text{Cl}$ - $0.5\text{Mg}(\text{NH}_2)_2$  was obtained. Hydrogen storage properties of  $\text{Li}_4(\text{NH}_2)_3\text{Cl}$ - $3\text{LiH}$  and  $\text{Li}_4(\text{NH}_2)_3\text{Cl}$ - $0.5\text{Mg}(\text{NH}_2)_2$ - $3\text{LiH}$  composites were evaluated between 200 °C and 300 °C. The onset of hydrogen release was reduced by 20 °C when  $\text{Li}_4(\text{NH}_2)_3\text{Cl}$ - $3\text{LiH}$  decomposed in the presence of  $\text{Mg}(\text{NH}_2)_2$  (180 °C with respect to 200 °C) and its hydrogen desorption rate increased by 83%. However, no change in the dehydrogenation activation energy was observed for  $\text{Li}_4(\text{NH}_2)_3\text{Cl}$ - $3\text{LiH}$  decomposition due to minor amounts of  $\text{Mg}(\text{NH}_2)_2$ . Hydrogen storage capacity under cycling was reduced from about 3.0 wt% to 1.5 wt% at 300 °C, after rehydrogenation at 6.0 MPa. The formation of  $\text{Li}_7(\text{NH})_3\text{Cl}$  was clearly identified in the dehydrogenated material. Unfortunately, the sloped plateau and the thermodynamic stability of the  $\text{Li}_4(\text{NH}_2)_3\text{Cl}$ - $3\text{LiH}$  precludes its hydrogen storage applicability.

### 1. Introduction

Hydrogen is an energy carrier and forms part of a renewable and sustainable energy system with use potential in hydrogen-fuelled vehicles. Currently, two of the most important aspects that remain to be resolved are the safety and the efficiency storage means. Many materials have shown good hydrogen absorption/desorption reversibility with high storage capacity. Light element complex hydrides such as alanates, amides and borohydrides are good materials for hydrogen storage.<sup>1-7</sup> Within these materials, the Li-N-H system can reversibly store hydrogen according to the following reaction between lithium imide and lithium amide:<sup>2</sup>



This system is considered to be suitable for hydrogen storage because its calculated enthalpy change ( $\Delta H$ ) is 45 kJ/mol and because, theoretically, it can release a relatively large amount of hydrogen of 6.5 wt% at 245 °C.<sup>3</sup> However, in spite of the potential of this system for reversible storage, there are still barriers for practical applications. In particular, the measured value of  $\Delta H$  (67 kJ/mol) is higher than the calculated possibly due to the ammonia emission, and the operational temperature is still too high due to thermodynamic and/or kinetic issues.<sup>7</sup> Thus it is necessary to lower

the reaction temperature. For this reason, the destabilization of  $\text{LiNH}_2$  was proposed,<sup>8,9</sup> where Li ions were partially substituted by elements with larger electronegativity, such as Mg.<sup>9-11</sup> Studies with different compositions or different starting materials for the Li-Mg-N-H system have been reported since 2004.<sup>10-16</sup>

David, *et al.* in 2007 found that increasing the  $\text{Li}^+$  mobility promotes the hydrogen sorption performance.<sup>17</sup> In this line, Matsuo *et al.*<sup>18</sup> found a new phase,  $\text{Li}_3(\text{NH}_2)_2\text{I}$  by mechanical milling and subsequent heat treatment of  $\text{LiNH}_2$  and  $\text{LiI}$ . This amide-halide presented ionic conductivities more than 1000 times greater than  $\text{LiNH}_2$ . More recently, Anderson *et al.* investigated the reaction of lithium amide with lithium/magnesium halides, which resulted in the formation of a series of amide-halide phases with rhombohedral or cubic structure, depending on the reaction time at 400 °C.<sup>19</sup> Moreover, they reported that the incorporation of halides into lithium amide enhanced the dehydrogenation behavior of the  $\text{LiNH}_2$ - $\text{LiH}$  system, which promoted the reduction/elimination of the ammonia as a by-product and also increased ionic conductivity with respect to  $\text{LiNH}_2$ .<sup>19,20</sup> However, the problem with the addition of halides is the reduction of the material gravimetric hydrogen capacity.

In a further study, two new amide-chlorides phases with lesser chloride content,  $\text{Li}_7(\text{NH}_2)_6\text{Cl}$  and  $\text{Li}_6\text{Mg}_{0.5}(\text{NH}_2)_6\text{Cl}$ , were synthesized.<sup>20,21</sup> The Mg-compound resulted in a mixture of rhombohedral and cubic phases, while a single phase was obtained for  $\text{Li}_7(\text{NH}_2)_6\text{Cl}$ . The hydrogen desorption of  $\text{Li}_7(\text{NH}_2)_6\text{Cl}$  with  $\text{LiH}$  was complete as previously reported for  $\text{Li}_4(\text{NH}_2)_3\text{Cl}$ .<sup>19</sup> It was showed in their work that the chloride ions were maintained into the structure after hydrogen desorption/absorption and therefore, the reaction could be reversible.<sup>21</sup> The imide rehydrogenation condition was carried out at 90 bar and 300 °C.<sup>21</sup> Moreover, the presence of

<sup>a</sup> Consejo Nacional de Investigaciones Científicas y Técnicas (CONICET), Av. Bustillo 9500, R8402AGP S.C. de Bariloche, Río Negro, Argentina. E-mail address: gamba.nadia@gmail.com; Fax: +54 294 4445190, Tel.: +54 294 4445712

<sup>b</sup> Centro Atómico Bariloche (CNEA), Argentina.

<sup>c</sup> Instituto Balseiro, Universidad Nacional de Cuyo, Argentina.

† Electronic Supplementary Information (ESI) available: See DOI: 10.1039/x0xx00000x

magnesium in the new composition showed no reduction of the desorption temperature with respect to the  $\text{Li}_3\text{Mg}_{0.5}(\text{NH}_2)_3\text{Cl}$  phase.<sup>20</sup> Although these materials are studied mainly because of its light-weight hydrogen storage properties, some of these materials might also have potential in other energy applications such as solid state lithium ion batteries, supercapacitors,  $\text{CO}_2$  capture and storage membranes.<sup>20</sup>

In other researches, the effect of the halides on the hydrogen storage properties of the Li-N-H and Li-Mg-N-H systems was also evidenced.<sup>16-27</sup> The effect of  $\text{MgCl}_2$  on the hydrogen desorption properties of the Li-N-H system was investigated and it was found that the addition of  $\text{MgCl}_2$  significantly improved the desorption properties, but it depended on the  $\text{MgCl}_2$  amount.<sup>23</sup> On the other hand, it was found that the addition of LiBr led to the formation of a  $\text{Li}_7(\text{NH}_2)_6\text{Br}$  phase, which promoted the migration of  $\text{Li}^+$  and improved the dehydrogenation kinetics of the Li-Mg-N-H system, while when adding LiCl, the dehydrogenation process observed was more complex and did not show significant improvements.<sup>25,26</sup> However, satisfactory results with the attempts of doping lithium amide with fluoride ions have not been achieved to date.<sup>22</sup>

Nevertheless, there is still no clear report of reversible hydrogen storage capacities for the amide-halide phases as well as the thermodynamic and kinetic properties so that they could be considered as a hydrogen storage system in practical applications. Therefore, the aim of this work is the synthesis of  $\text{Li}_4(\text{NH}_2)_3\text{Cl}$ -3LiH and  $\text{Li}_3\text{Mg}_{0.5}(\text{NH}_2)_3\text{Cl}$ -3LiH composites by mechanical milling and the study of their hydrogen storage properties. For this purpose,  $\text{Li}_4(\text{NH}_2)_3\text{Cl}$  and  $\text{Li}_3\text{Mg}_{0.5}(\text{NH}_2)_3\text{Cl}$  compositions were prepared by mechanical milling of  $\text{LiNH}_2$  with LiCl or  $\text{MgCl}_2$ , respectively. Kinetic and thermodynamic properties of the reaction of both amide-chloride composites with LiH were investigated. The role of the addition of chloride ions on the hydrogen desorption properties was analysed. The synthesis conditions, the dehydrogenation kinetics and the structural/thermal study of the composites before and after de/hydrogenation cycles are reported below.

## 2. Experimental

### 2.1. Sample synthesis

The following compounds  $\text{Li}_4(\text{NH}_2)_3\text{Cl}$  and  $\text{Li}_3\text{Mg}_{0.5}(\text{NH}_2)_3\text{Cl}$  were prepared by milling of  $\text{LiNH}_2$  with LiCl or  $\text{MgCl}_2$ , respectively. To obtain the  $\text{Li}_4(\text{NH}_2)_3\text{Cl}$  compound, the first step was the milling of  $\text{LiNH}_2$  (Sigma-Aldrich, purity  $\geq 98\%$ ) and LiCl (Sigma-Aldrich, purity  $\geq 99\%$ ) powders in a molar ratio of 3:1. The milling procedure was performed in a Fritsch P6 planetary mill under a 0.1 MPa of argon atmosphere at 400 rpm (ball to powder ratio of 60:1). The total time of the milling was of 5 h. To avoid temperature ramping during milling, there was a 15-minute pause for each 10-minute run. The second step was the milling of pre-milled 3LiNH<sub>2</sub>-LiCl with LiH (Fluka, 95%) in a 1:3 molar ratio at 400 rpm for additional time of 3 h under 0.1 MPa of Ar. The obtained sample was submitted to thermal treatment at 200 °C for 0.5 h and 20 h under 6.0 MPa of hydrogen pressure. The final sample was indicated as Li composite.

By comparison the  $\text{Li}_3\text{Mg}_{0.5}(\text{NH}_2)_3\text{Cl}$ -LiH composite was prepared using  $\text{LiNH}_2$  and anhydrous  $\text{MgCl}_2$  (Sigma-Aldrich, purity  $\geq 98\%$ ) as starting materials in a molar ratio of 6:1. The pre-milled sample was mixed with LiH by milling in a 1:3 molar ratio at 400 rpm for 3 h under 0.1 MPa of Ar. The final composite was heated at 200 °C for

0.5 h and 20 h under 6.0 MPa of  $\text{H}_2$  and indicated as Li-Mg composite.

All sample-handling operations, before and after milling, were performed under an inert atmosphere of high purity argon in a MBraun Unilab glove box with a circulative purification system. Oxygen and moisture levels were kept below 1 ppm during operations to avoid the degradation of the samples.

### 2.2. Sample characterization

The structural analysis of the different samples was performed through X-ray powder diffraction (XRPD, PANalytical Empyrean equipment) and Fourier transform infrared spectroscopy (FTIR, PerkinElmer Spectrum 400). For the XRPD measurements, it was used  $\text{CuK}\alpha$  radiation (voltage of 40 kV, a current of 30 mA and graphite monochromator) in the range of  $2\theta=10^\circ\text{-}80^\circ$  with  $0.02^\circ$  step size and 3 seconds for step. During the XRPD data collection the samples were maintained under argon atmosphere to prevent the reaction with oxygen and humidity using a tightly sealed sample holder, with mylar windows. The IR spectra were obtained in the  $800\text{-}4000\text{ cm}^{-1}$  wave number range at room temperature. Pellets with samples and dry KBr were done in the glove box and then closed into a de-mountable cell holder with KBr plates to prevent the reaction of the samples with the air. FTIR was also used to analyse the gases released during the dehydrogenation of the samples. The gaseous phase was collected in a degassed quartz optical cell with KBr windows and the gas phase spectra were taken at room temperature.

Differential scanning calorimetry (DSC, TA 2910 calorimeter) under an Ar atmosphere was used to study the thermal behaviour of the samples. The flow rate of Ar was  $122\text{ ml min}^{-1}$  and the heating rate of  $5\text{ }^\circ\text{C min}^{-1}$  for routine analysis. About 3-5 mg of samples were transferred into aluminium capsules in the glove box. The Kissinger method was employed to determine the activation energy of the hydrogenation process ( $E_{\text{app}}$ ) according to the equation (2),<sup>28</sup> where  $T_p$  is the peak temperature of the endothermic event,  $\beta$  is the heating rate,  $E_{\text{app}}$  is the apparent activation energy and  $R$  is the ideal gas constant.

$$\frac{d[\ln(\frac{\beta}{T_p^2})]}{d(\frac{1}{T_p})} = \frac{-E_{\text{app}}}{R} \quad (2)$$

The  $T_p$  was obtained from the DSC curves at heating rates of 1, 2, 5, 10 and  $15\text{ }^\circ\text{C min}^{-1}$  and the slope of the fitted line ( $\ln(\beta/T_p^2)$  vs.  $1/T_p$ ) corresponds to the activation energy of the reaction.

The curves of pressure composition isotherm (PCI), hydrogen sorption kinetics and desorption-absorption capacities were obtained using a modified Sieverts-type device, coupled with a mass flow controller. A known mass sample was transferred into a stainless steel reactor in the glove box and then the reactor connected to the Sieverts apparatus. For hydrogen desorption PCI measurement, a programmed amount of hydrogen was extracted from the system through the mass flow controller in each step. The criteria used to determine the equilibrium condition of the system

was either keeping the temporal variation of pressure lower than a fixed value or waiting for a given amount of time. When one of these criteria was met, it was considered that the system was in equilibrium and a point in the PCI curve was saved. Then, the software started the following equilibrium point using again the mass flow controller.

Isothermal dehydrogenation experiments were measured at 200 °C and 300 °C under 0.02 MPa of hydrogen pressure. The sample was heated up to the reaction temperature under hydrogen pressure (6.0 MPa) and kept at this temperature for 30 min before each dehydrogenation measurement. The rehydrogenation process was performed with 6.0 MPa of hydrogen using a mass flow controller during the measuring time. On the other hand, non-isothermal dehydrogenation experiments were measured from 20 °C to 300 °C with heating rate of 5 °C min<sup>-1</sup> and 0.02 MPa of hydrogen pressure. The absorbed/desorbed hydrogen amount was reported as wt% with respect to the total mass.

### 3. Results and Discussion

#### 3.1 New synthesis procedure of Li<sub>4</sub>(NH<sub>2</sub>)<sub>3</sub>Cl-type phases

With the aim to synthesize Li<sub>4</sub>(NH<sub>2</sub>)<sub>3</sub>Cl and Li<sub>3</sub>Mg<sub>0.5</sub>(NH<sub>2</sub>)<sub>3</sub>Cl phases, mixtures of LiNH<sub>2</sub> with LiCl or MgCl<sub>2</sub> (3:1 and 6:1 molar ratio, respectively) were first milled under argon for 5 h. In the case of the LiCl addition, no evidence of the reaction during milling was detected. On the contrary, LiNH<sub>2</sub> reacted with MgCl<sub>2</sub> forming LiCl and a mixture of LiNH<sub>2</sub> (main phase)-Mg(NH<sub>2</sub>)<sub>2</sub> (minority phase), as detected by XRPD and FTIR respectively (see supplementary material, Fig. S1). The formation of Mg(NH<sub>2</sub>)<sub>2</sub> by milling of LiNH<sub>2</sub> and MgCl<sub>2</sub> was in agreement with our previous work.<sup>16</sup> However, in the present case the formation of Mg(NH<sub>2</sub>)<sub>2</sub> occurred in the presence of an excess of LiNH<sub>2</sub>, according to following reaction (Eqn. 3):

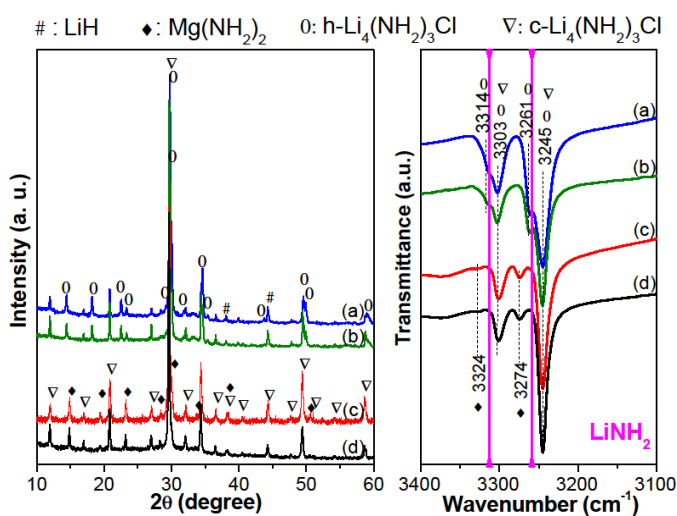
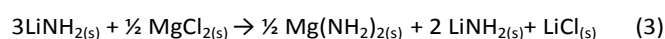
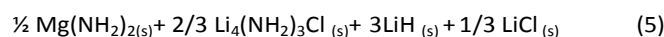
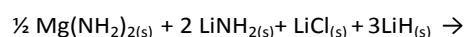
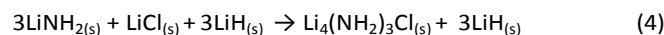


**Figure 1.** XRPD (A) and FTIR (B) of the Li (a, b) and Li-Mg (c, d) composites, treated at 200 °C and 6.0 MPa for: (a, c) 0.5 h (b, d) 20 h.

After ball-milling of LiNH<sub>2</sub> with the different metal chlorides, 3LiH was added and the final samples were thermal-treated under 6.0 MPa of hydrogen pressure for 0.5 h at 200 °C. XRPD patterns (Fig. 1A) show the formation of the amide chloride phases and the simultaneous presence of LiH. These patterns resemble those of the Li<sub>4</sub>(NH<sub>2</sub>)<sub>3</sub>Cl formed by direct reaction of LiNH<sub>2</sub> and LiCl during heating at 400 °C under argon without previous milling.<sup>19</sup> For the mixture 3LiNH<sub>2</sub>-LiCl, both cubic and hexagonal Li<sub>4</sub>(NH<sub>2</sub>)<sub>3</sub>Cl phases were clearly identified. In the case of 3LiNH<sub>2</sub>-0.5MgCl<sub>2</sub>, the most intense peaks from the cubic Li<sub>4</sub>(NH<sub>2</sub>)<sub>3</sub>Cl phase as well as the Mg(NH<sub>2</sub>)<sub>2</sub> were recognized. The reactions can be expressed as:



FTIR in Fig.1B confirms the formation of the Li<sub>4</sub>(NH<sub>2</sub>)<sub>3</sub>Cl phase by the identification of their characteristic bands at 3303 and 3245 cm<sup>-1</sup>. Moreover, the presence of shoulders at 3314 and 3261cm<sup>-1</sup> was previously associated with the hexagonal Li<sub>4</sub>(NH<sub>2</sub>)<sub>3</sub>Cl structure,<sup>19,20</sup> which are also coincident with the LiNH<sub>2</sub> bands. The 3LiNH<sub>2</sub>-0.5MgCl<sub>2</sub>-3LiH mixture also shows the typical N-H vibrations at 3324 and 3274 cm<sup>-1</sup> belonging to Mg(NH<sub>2</sub>)<sub>2</sub>.

To evaluate the thermal stability of the Li<sub>4</sub>(NH<sub>2</sub>)<sub>3</sub>Cl phases obtained by the new synthesis route, an additional thermal treatment was performed for 20 h at 200 °C, and the final solid analysed by XRPD and FTIR. It can be seen from curves (b) and (d) in Figs. 1A and B that the additional thermal treatment did not introduce visible structural modifications in the samples. This structural study is a confirmation of the thermal stability of the final phases at 200 °C under hydrogen pressure. As a novel result, the proposed synthesis procedure allowed the formation of Li<sub>4</sub>(NH<sub>2</sub>)<sub>3</sub>Cl, even when the starting mixture had the composition to obtain Li<sub>3</sub>Mg<sub>0.5</sub>(NH<sub>2</sub>)<sub>3</sub>Cl. Apparently, under the experimental conditions of this study, the formation Li<sub>4</sub>(NH<sub>2</sub>)<sub>3</sub>Cl is favoured with respect to Li<sub>3</sub>Mg<sub>0.5</sub>(NH<sub>2</sub>)<sub>3</sub>Cl. In addition, a mixture of cubic and hexagonal Li<sub>4</sub>(NH<sub>2</sub>)<sub>3</sub>Cl phases were obtained for the Li composite at 200 °C, whereas only the cubic one was formed after prolonged heating for the Li-Mg composite. In the following section, the products of reactions (4) and (5) were evaluated as potential hydrogen storage materials.

#### 3.2 Dehydrogenation/hydrogenation properties of amide-chloride samples

To elucidate the decomposition behaviour of the Li composite, the as-synthesized samples were studied during non-isothermal DSC and volumetric measurements (Figure 2). DSC revealed that the onset dehydrogenation was reduced in 20 °C when the Li composite decomposes in the presence of Mg(NH<sub>2</sub>)<sub>2</sub> (180 °C with respect to 200 °C). In addition, the shapes of DSC curves were different: for the Li<sub>4</sub>(NH<sub>2</sub>)<sub>3</sub>Cl, a single and wide peak, whereas for the Li<sub>4</sub>(NH<sub>2</sub>)<sub>3</sub>Cl in presence of Mg(NH<sub>2</sub>)<sub>2</sub> consists of a narrow peak with a shoulder,

indicating a distinct increase in the reaction rate. Volumetric measurements confirm the behaviour observed in DSC experiments (Fig. 2B). As shown in Fig. 2B, for the  $\text{Li}_4(\text{NH}_2)_3\text{Cl}$  decomposition, a single hydrogen desorption process is noted. When the sample contained  $\text{Mg}(\text{NH}_2)_2$ , an apparent stepwise dehydrogenation process occurred. By comparison with the Li composite decomposition curve, the beginning of hydrogen release could be associated with the  $\text{Mg}(\text{NH}_2)_2$  decomposition followed by the  $\text{Li}_4(\text{NH}_2)_3\text{Cl}$ . In addition, the volumetric curve shifts to lower temperature, providing further evidence for the reduction of the dehydrogenation temperature due to  $\text{Mg}(\text{NH}_2)_2$ . The extent of the dehydrogenation accounted for 2.9 and 3.5 wt% for the  $\text{Li}_4(\text{NH}_2)_3\text{Cl}$  without and with  $\text{Mg}(\text{NH}_2)_2$  presence, respectively. These values are lower than the theoretical hydrogen storage capacity of each composite (about 4.4 wt% of hydrogen). No emission of  $\text{NH}_3$  was detected during the dehydrogenation up to 300 °C, which suggests a suppression of ammonia emission due to amide-halide presence, in a similar way to previous works.<sup>18</sup> Davies *et al.*<sup>18</sup> using TPD measurements characterized the hydrogen release of the  $\text{Li}_4(\text{NH}_2)_3\text{Cl}$ ,  $\text{Li}_7(\text{NH}_2)_6\text{Cl}$  and  $\text{Li}_6\text{Mg}_{0.5}(\text{NH}_2)_6\text{Cl}$  materials. They found that the onset hydrogen desorption temperature was not modified due to the presence of  $\text{Mg}^{2+}$  or due to the use of different stoichiometric ratios between  $\text{Li}^+$  and  $\text{NH}_2^-$ . In addition, the dehydrogenation occurred at higher temperatures (300 °C) than those obtained in the present work (Fig. 2).

This different behaviour could be associated with the synthesis procedure developed to produce  $\text{Li}_4(\text{NH}_2)_3\text{Cl}$ . The mild conditions used in our synthesis procedure, i.e. milling at room temperature followed by heating at low temperature (200 °C), could induce the production of favourable material microstructure for the dehydrogenation (small crystal and particle size, higher surface area, etc.).

Figure 3 displays the isothermal dehydrogenation curves of the Li composite at different temperatures. At 200 °C, the dehydrogenation from the Li composite was practically undetectable after 1 h, which suggests a thermodynamic limitation (Fig. 3A). Due to the undetectable first dehydrogenation, no second hydrogen cycling was performed. As the temperature increased to 300 °C, the Li composite released about 2.9 wt% of hydrogen (Fig. 3B). As a difference, the Li-Mg composite shows 1.5 wt% of hydrogen releasing at 200 °C (Fig. 3A), which is in agreement with the theoretical value obtained supposing that all  $\text{Mg}(\text{NH}_2)_2$  formed decomposes to  $\text{Li}_2\text{Mg}(\text{NH}_2)_2$  (according to eqn. 4). Moreover, at 300 °C, 3 wt% of hydrogen could be desorbed fast after 0.5 h (Fig. 3B). By analysing the slope between 0.02 wt% and 0.15 wt% of the isothermal dehydrogenation curve at 300 °C, the hydrogen desorption rate of the sample containing Mg was calculated to be  $2.7 \pm 0.1$  wt% per min, which is an 83 % increase with respect to that of  $\text{Li}_4(\text{NH}_2)_3\text{Cl}$ -3LiH ( $0.46 \pm 0.01$  wt%  $\text{min}^{-1}$ ).

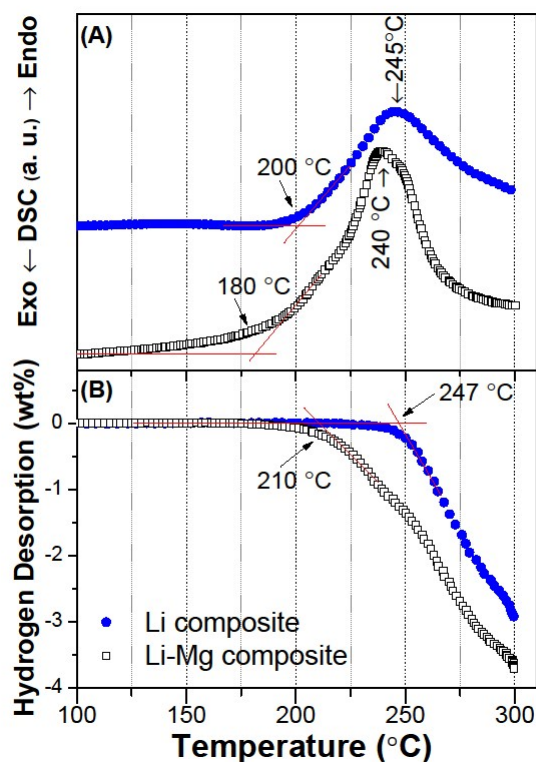


**Figure 2.** DSC (A) and hydrogen volumetric release (B) curves of the Li and Li-Mg composites.

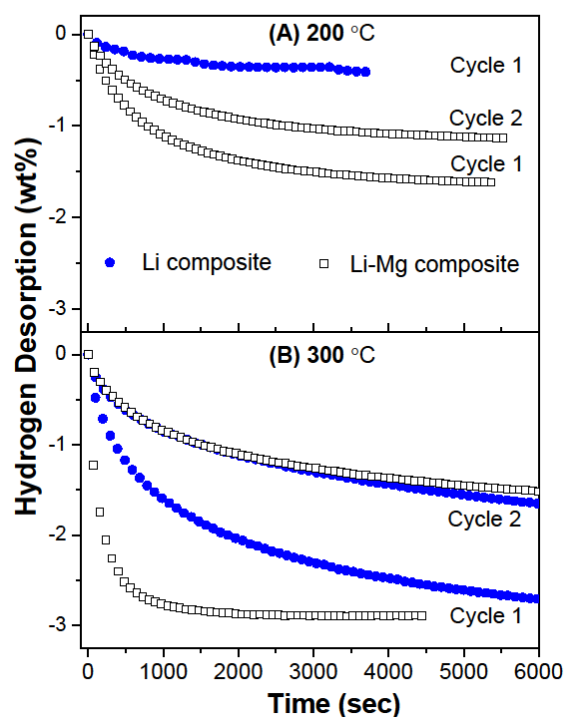


**Figure 3.** Dehydrogenation curves of Li and Li-Mg composites at (A) 200 °C, (B) 300 °C.

Clearly, the presence of Mg in the composite improves the dehydrogenation behaviour with respect to the Li-based composite. To evaluate hydrogen storage reversibility, the dehydrogenated composites were rehydrogenated at 200 °C and 300 °C under 6.0 MPa of hydrogen pressure. The second dehydrogenated cycles are also shown in Fig. 3. As a general behaviour, the second dehydrogenation cycle displays deterioration in the kinetics with respect to the first cycle. In fact, during the first cycle, 3 wt% was released after 2.5 h and 0.5 h for Li and Mg-based composites, respectively, whereas for the second dehydrogenation, about 1.5 wt% of hydrogen release required 2.5 h in both cases.

A combination of XRPD and FTIR was used to analyse the nature of the dehydrogenated and rehydrogenated phases. Figure 4A shows the XRPD patterns after non-isothermal dehydrogenation up to 300 °C for both composites. In the case of the Li composite, the final phase resembles the one reported previously by Anderson *et al.*<sup>19</sup> and it was identified as cubic  $\text{Li}_7(\text{NH})_3\text{Cl}$ . A similar phase was also observed after the dehydrogenation of Li-Mg composite together with an excess of LiCl (see eqn. 4). For the Li-Mg composite, no evidence of the presence of any Mg containing phase was detected by XRPD. However, some extension of Mg substitution in the imide-chloride structure cannot be ruled out. Additional structural characterization by FTIR (Fig. 4B) confirms the imide nature of the main dehydrided phase by the band at  $3163\text{ cm}^{-1}$ . Moreover, in the case of the Li composite, the bands at  $3303\text{-}3297$  and  $3244\text{ cm}^{-1}$  are also observed. The bands evidence uncompleted dehydrogenation of Li composite.

The structural modifications of the composites were also studied after an isothermal hydrogen cycling. Figures 5A and 5B show the XRPD patterns and FTIR spectra, respectively, of the Li and Li-Mg composite before the 1<sup>st</sup> dehydrogenation,

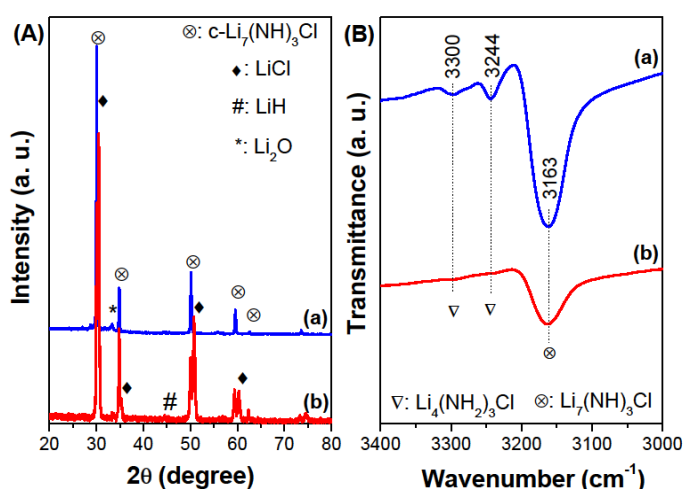


**Figure 4.** (A) XRPD patterns and (B) FTIR spectra of the Li (a) and Li-Mg (b) composites after non-isothermal dehydrogenation.

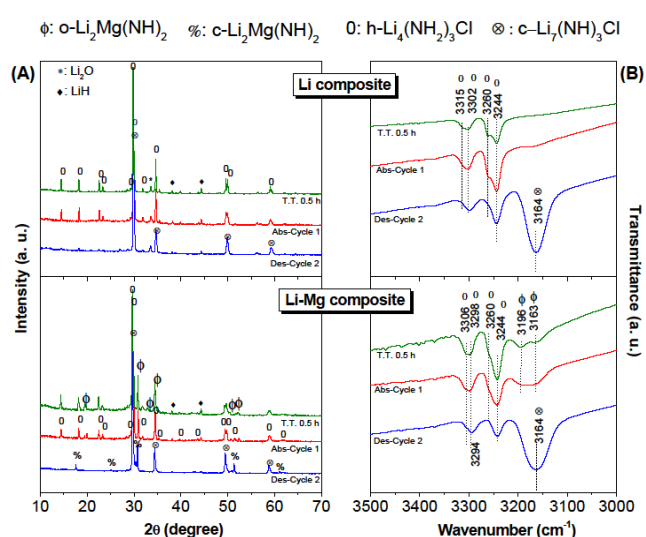
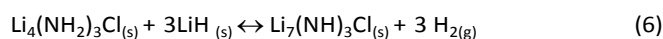


**Figure 5.** XRPD patterns (A) and FTIR spectra (B) of Li and Li-Mg composites after treatment at 300 °C under 0.6 MPa, 1<sup>st</sup> rehydrogenation and 2<sup>nd</sup> dehydrogenation.

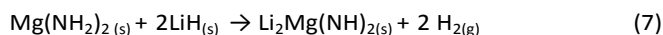
after the 1<sup>st</sup> rehydrogenation and the 2<sup>nd</sup> dehydrogenation cycles. In the case of the Li composite, the heating at 300 °C under 6.0 MPa of hydrogen pressure induced the cubic to hexagonal phase transition of  $\text{Li}_4(\text{NH}_2)_3\text{Cl}$ , as it can be inferred by comparison with Fig. 1. In addition, after rehydrogenation, only a hexagonal  $\text{Li}_4(\text{NH}_2)_3\text{Cl}$  phase was detected (see Fig. 5A and 5B), while the dehydrogenation conducted to uncompleted decomposition of the  $\text{Li}_4(\text{NH}_2)_3\text{Cl}$  and the  $\text{Li}_7(\text{NH})_3\text{Cl}$  formation. For the Li-Mg composite, a decomposition of a minor amount of  $\text{Mg}(\text{NH}_2)_2$  to orthorhombic  $\text{Li}_2\text{Mg}(\text{NH})_2$  occurred during heating at 300 °C under 6.0 MPa of hydrogen pressure, as it is inferred by the bands at  $3196$  and  $3163\text{ cm}^{-1}$ . In addition, in a similar way to the Li-composite, a complete cubic-hexagonal  $\text{Li}_4(\text{NH}_2)_3\text{Cl}$  phase transition occurred at 300 °C under 6.0 MPa of hydrogen pressure. After the 1<sup>st</sup> rehydrogenation, the presence of  $\text{o-Li}_2\text{Mg}(\text{NH})_2$  and the hexagonal  $\text{Li}_4(\text{NH}_2)_3\text{Cl}$  phase was detected (Fig. 5A and 5B). This result indicates that  $\text{Li}_2\text{Mg}(\text{NH})_2$  cannot be rehydrogenated under the used experimental conditions. Finally, the 2<sup>nd</sup> dehydrogenation cycle led to the formation of  $\text{Li}_7(\text{NH})_3\text{Cl}$  and cubic- $\text{Li}_2\text{Mg}(\text{NH})_2$ . A good agreement between FTIR assignments and XRPD was found in each stage of the hydrogen cycling. It is interesting to remark that during the hydrogen cycling of the Mg-composite, a progressive widening in the band position of  $\text{Li}_4(\text{NH}_2)_3\text{Cl}$  from  $3303\text{ cm}^{-1}$  to  $3294\text{ cm}^{-1}$  is observed. Although it could be partially associated with the Mg incorporation into the  $\text{Li}_4(\text{NH}_2)_3\text{Cl}$  structure, the observation of a similar shift of the  $3303\text{ cm}^{-1}$  for the Li-composite suggests some kind of disorder in the N-H bond.

Considering the structural modifications identified during hydrogen cycling, the reversible reaction for both composites can be expressed as:



In the case of the Li composite, decomposition was uncompleted under both isothermal and non-isothermal conditions. It was confirmed by the detection of  $\text{Li}_4(\text{NH}_2)_3\text{Cl}$  by XRPD and FTIR at the end of the dehydrogenation.

Moreover, the simultaneous presence of  $\text{LiNH}_2$  in the hydrogenated composite from the beginning of the synthesis procedure could not be ruled out, because the bands in FTIR have the same positions as those reported for the hexagonal  $\text{Li}_4(\text{NH}_2)_3\text{Cl}$ . On the other hand, the  $\text{Mg}(\text{NH}_2)_2$  decomposition in the Li-Mg composite occurred during heating at 300 °C under 6.0 MPa of hydrogen, according to the reaction:



This reaction could be responsible for the improved dehydrogenation kinetics of the Li-Mg composite with respect to the Li composite. Moreover, while under non-isothermal conditions a complete decomposition of  $\text{Li}_4(\text{NH}_2)_3\text{Cl}$  and  $\text{Mg}(\text{NH}_2)_2$  occurred, a partial dehydrogenation of  $\text{Li}_4(\text{NH}_2)_3\text{Cl}$  was noted under isothermal conditions. In the next section, kinetic and thermodynamic properties of Li composite will be analyzed to clarify the effect of minor amounts of  $\text{Mg}(\text{NH}_2)_2$  on the dehydrogenation kinetics and to establish the hydrogen storage properties of the lithium amide-chloride phase.

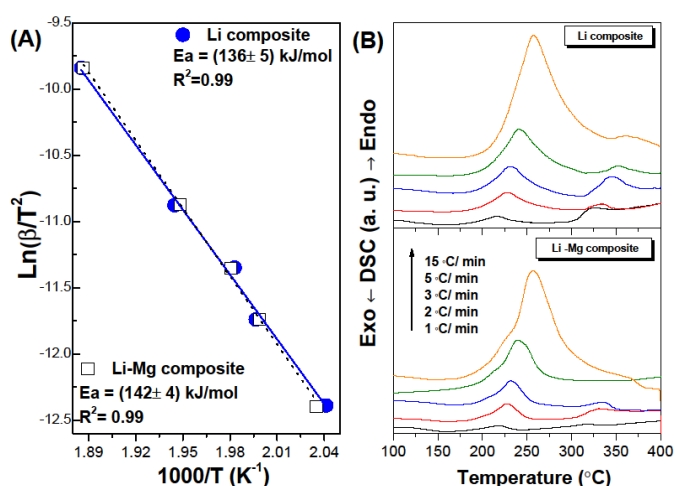
### 3.3 Thermodynamics and kinetics of the $\text{Li}_4(\text{NH}_2)_3\text{Cl}$ -3LiH composites

It was shown in fig. 2A that the dehydrogenation process of the  $\text{Li}_4(\text{NH}_2)_3\text{Cl}$  containing composites is endothermic, implying that hydrogen storage should be thermodynamically reversible. On the other hand, it was also observed that the Li-Mg composite displays faster dehydrogenation with respect to the Li composite. In this context, it is relevant to evaluate the kinetic barrier for dehydrogenation as well as the thermodynamic stability of the composites.

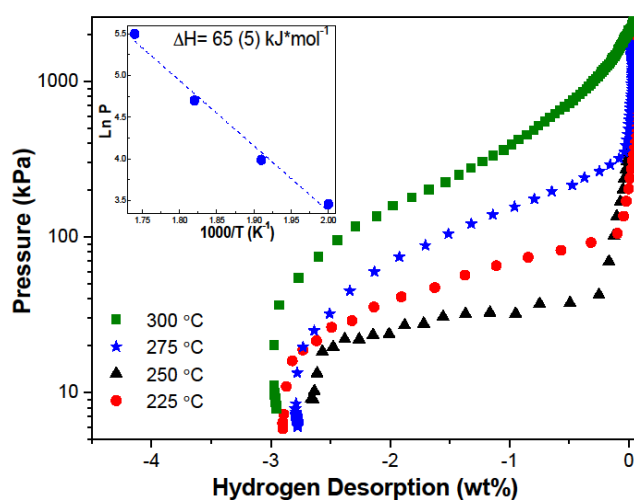
Figure 6 shows the Kissinger plots (Fig. 6A) and the DSC curves (Fig. 6B) obtained at different heating rates for the Li (Fig. 6A) and Li-Mg composites. Using the Kissinger plot, from the slope of the straight lines, the activation energy  $E_{\text{app}}$  calculated was  $136 \pm 5$  kJ/mol  $\text{H}_2$  and  $142 \pm 4$  kJ/mol  $\text{H}_2$  for Li and Li-Mg composites, respectively. It can be seen that the values calculated for  $E_{\text{a}}$  are about the same order. This is in agreement with the identification of  $\text{Li}_4(\text{NH}_2)_3\text{Cl}$  by FTIR instead of  $\text{Li}_3\text{Mg}_{0.5}(\text{NH}_2)_3\text{Cl}$ . Apparently, the presence of  $\text{Mg}(\text{NH}_2)_2$  in the composite as a minority phase, has no influence on the kinetic barrier of dehydrogenation. The activation energy values are similar to those obtained in our previous work during the decomposition study of an  $\text{Mg}(\text{NH}_2)_2$ -2LiH-2LiCl sample.<sup>16</sup>

Figure 7 shows dehydrogenation PCIs at different temperatures for the Li composite. The PCI at 225 °C displays a relatively flat plateau, with a value of hydrogen pressure of about ~32 kPa. At higher temperatures, the PCI curves display sloped plateaus in the complete dehydrogenation range, with hydrogen desorption capacities of 2.7 wt % and 2.9 wt % at 250 and 300 °C, respectively. The wide variation in the hydrogen equilibrium pressure along the plateau, e.g. from 1000 to 100 kPa in the worst situation at 300 °C, is an important limitation for hydrogen storage applications. The sloping behaviour in PCI curves was previously observed for the Li-N-H system and could be interpreted considering that different phases with intermediate stoichiometry exist between  $\text{LiNH}_2$  and  $\text{Li}_2\text{NH}$ .<sup>17,29</sup> A similar behaviour was recently observed for  $\text{LiNH}_2$ -LiH doped with different amounts of  $\text{AlCl}_3$ , where a Li-Al-N-H-Cl phase isostructural with  $\text{Li}_4(\text{NH}_2)_3\text{Cl}$  was formed.<sup>27</sup>

To determine the decomposition enthalpy of  $\text{Li}_4(\text{NH}_2)_3\text{Cl}$ -3LiH, equilibrium hydrogen pressures at each temperature were determined from PCI curves in the middle of the plateau.



**Figure 6:** (A) Kissinger plot and (B) DSC curves for the Li and Mg-based composites.



**Figure 7:** Dehydrogenation PCI curves of Li composite at different temperatures. Inset plot: Van't Hoff plot.

The values obtained were: 32 kPa at 225 °C, 54 kPa at 250 °C, 110 kPa at 275 °C and 245 kPa at 300 °C.

The Van't Hoff plot derived from these equilibrium pressures at different temperatures is shown in the inset plot of Fig. 7. The dehydrogenation enthalpy calculated for the Li composite is  $(65 \pm 5)$  kJ mol<sup>-1</sup>. This value is different if the estimation is performed at the beginning or at the end of the plateau. However, independently of the enthalpy value obtained, the equilibrium pressure at a fixed temperature for Li composite is lower than that for Mg(NH<sub>2</sub>)<sub>2</sub>-2LiH, but it is similar to that for the LiNH<sub>2</sub>-LiH system.<sup>27,30</sup> Therefore, taking into account that the reversibility of the Li composite is limited, the PCI measurements provide evidence of major thermodynamic stability of Li<sub>4</sub>(NH<sub>2</sub>)<sub>3</sub>Cl with respect to Mg(NH<sub>2</sub>)<sub>2</sub> and the operating pressure at each temperature involving a wide range, it is possible to conclude that the Li composite possesses strong limitations to be applied as hydrogen storage material.

#### 4. Conclusions

A new synthesis procedure was developed to produce Li<sub>4</sub>(NH<sub>2</sub>)<sub>3</sub>Cl and Li<sub>3</sub>Mg<sub>0.5</sub>(NH<sub>2</sub>)<sub>3</sub>Cl from the milling of LiNH<sub>2</sub> with LiCl or MgCl<sub>2</sub>. After ball-milling, 3LiH was added and the final material was thermally treated at 200 °C under 6.0 MPa of hydrogen. Independently of the metal chloride used in the starting sample, successful synthesis of Li<sub>4</sub>(NH<sub>2</sub>)<sub>3</sub>Cl was accomplished. No evidence of the Li<sub>3</sub>Mg<sub>0.5</sub>(NH<sub>2</sub>)<sub>3</sub>Cl formation was detected from the ball-milling of LiNH<sub>2</sub>-0.5MgCl<sub>2</sub>; in fact, minor amounts of Mg(NH<sub>2</sub>)<sub>2</sub> were produced by a metathesis reaction between LiNH<sub>2</sub> and MgCl<sub>2</sub>.

Hydrogen storage properties of the Li<sub>4</sub>(NH<sub>2</sub>)<sub>3</sub>Cl-3LiH and Li<sub>4</sub>(NH<sub>2</sub>)<sub>3</sub>Cl-0.5Mg(NH<sub>2</sub>)<sub>2</sub>-3LiH composites were characterized using isothermal and non-isothermal measurements. Dehydrogenation temperature was reduced by 20 °C when Li<sub>4</sub>(NH<sub>2</sub>)<sub>3</sub>Cl-3LiH decomposed in the presence of Mg(NH<sub>2</sub>)<sub>2</sub>. In addition, hydrogen desorption kinetics was improved due to the presence of Mg(NH<sub>2</sub>)<sub>2</sub>. However, the activation energy of dehydrogenation was about the same for both composites (~140 kJ/mol), suggesting that the kinetic limiting factor is associated with the Li<sub>4</sub>(NH<sub>2</sub>)<sub>3</sub>Cl phase. During hydrogen cycling, the reversibility reaction involved the formation of Li<sub>7</sub>(NH)<sub>3</sub>Cl in the dehydrogenated state and the rehydrogenation of Li<sub>4</sub>(NH<sub>2</sub>)<sub>3</sub>Cl. However, the hydrogen storage capacity decreased with hydrogen cycling from 3.0 wt% to 1.5 wt% of hydrogen at 300 °C and 6.0 MPa. Regarding thermodynamic properties, PCIs determined in the temperature range between 225 °C and 300 °C showed a sloped plateau. Using equilibrium pressure at the middle of the plateau the decomposition enthalpy calculated was  $(65 \pm 5)$  kJ mol<sup>-1</sup>. Independently of the enthalpy value, the Li<sub>4</sub>(NH<sub>2</sub>)<sub>3</sub>Cl-3LiH composite displays higher thermodynamic stability than Mg(NH<sub>2</sub>)<sub>2</sub>-2LiH and a similar one to the LiNH<sub>2</sub>-LiH system. Therefore, the Li<sub>4</sub>(NH<sub>2</sub>)<sub>3</sub>Cl-3LiH composite possesses limited kinetic and thermodynamic properties to be considered as a potential material for hydrogen storage applications. Further studies are currently

under development to evaluate the thermodynamic and kinetic behaviour of analogous amide-halide compounds.

#### Acknowledgements

This study has been partially supported by CONICET (National Council of Scientific and Technological Research), CNEA (National Commission of Atomic Energy), ANPCyT (PICT N° 1052) and Instituto Balseiro (University of Cuyo). We would also like to thank the Department of Characterization of Materials for the XRPD devices. The authors thank to Adrián Borrelli for the English revision of the manuscript.

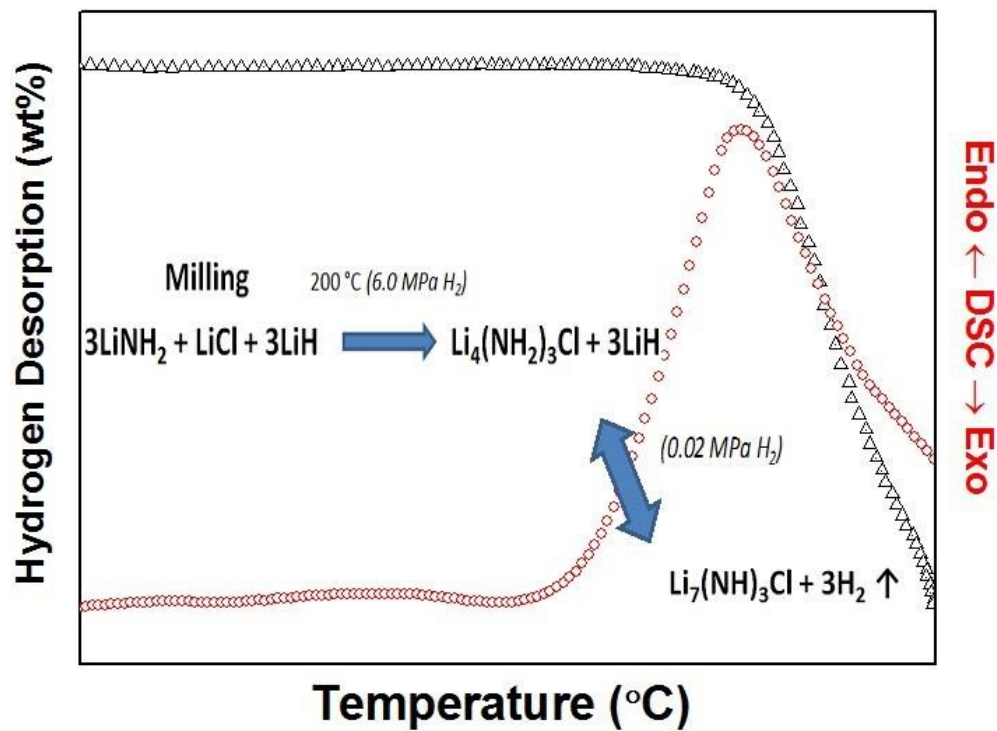
#### References

- B. Bogdanović and M. Schwickardi, *J. Alloys Compd.*, 1997, **253**, 1.
- P. Chen, Z.T. Xiong, J. Luo, J. Lin, K.L. Tan, *Nature* 2002, 420, 302.
- P.Chen, Z.T. Xiong, J. Luo, J. Lin, K.L. Tan, *J. Phys. Chem. B* 2003, **107**, 10967.
- Xiong, Z. T., Hu, J. J., Wu, G. T., Chen, P., Luo, W. F.; Gross, K.; Wang, J. *J. Alloys Compd.*, 2005, **398**, 235.
- H.-W. Li, Y. Yan, S. Orimo, A. Züttel and C. M. Jensen, *Energies*, 2011, **4**, 185.
- S. Orimo, Y. Nakamori, J. R. Eliseo, A. Züttel, C. M. Jensen, *Chem. Rev.*, 2007, **107**, 4111.
- S. Isobe, T. Ichikawa, K. Tokoyoda, N. Hanada, H. Leng, H. Fujii and Y. Kojima, *Thermochim. Acta*, 2008, **468**, 35.
- S.V. Alapati, J. K. Johnson, D.S. Sholl, *J. Phys. Chem. B*, 2006, **110**, 8769.
- J. J. Vajo, G. L. Olson, *Scripta Mater.*, 2007, **56**, 829.
- W. Luo, *J. Alloys Compd.*, 2004, **381**, 284.
- H. Leng, T. Ichikawa, S. Hino, T. Nakagawa, H. Fujii, *J. Phys. Chem. B*, 2005, **109**, 10744.
- Y. Liu, J. Hu, Z. Xiong, G. Wu, *J. Mater. Res.*, 2007, **22**, 1339
- R. R. Shahi, H. Raghubanshi, M.A. Shaz, O.N. Srivastava, *Int. J. Hydrogen Energy*, 2013, **38**, 8863.
- B. Zhang, Y. Wu, *J Alloys Compd.*, 2014, **613**, 199.
- R. Parviz, R.A. Varin, *Int. J. Hydrogen Energy*, 2001, **38**, 8313.
- N. S. Gamba, P. Arneodo Larochette and F. C. Gennari, *RSC Adv.*, 2015, **5**, 68542.
- W. I. F. David, M. O. Jones, D. H. Gregory, C. M. Jewell, S. R. Johnson, A. Walton, *J. Am. Chem. Soc.*, 2007, **129**, 1594.
- M. Matsuoto, T. Sato, Y. Miura, H. Oguchi, Y. Zhou, H. Maekawa, H. Takamura, S. Orimo, *Chem. Mater.*, 2010, **22**, 2702.
- P. A. Anderson, P. A. Chater, D. R. Hewett, P. R. Slater, *Faraday Discuss.*, 2011, **151**, 271.
- R. A Davies, D. R Hewett and P. A Anderson, *Adv. Nat. Sci.: Nanosci. Nanotechnol.*, 2015, **6**, 015005.
- R. A. Davies, P. A. Anderson, *Int. J. Hydrogen Energy*, 2015, **40**, 3001.
- R. A. Davies, D. R. Hewett, E. Korkiakoski, S. P. Thompson, P. A. Anderson, *J. Alloys Compd.*, 2015, **645**, S343.
- H. Leng, Z. Wua, W. Duan, G. Xia, Z. Li, *Int. J. Hydrogen Energy*, 2012, **37**, 903.
- C. Price, J. Gray, R. Lascola Jr., D. L. Anton, *Int. J. Hydrogen Energy*, 2012, **37**, 2742.
- B. Li, Y. Liu, C. Li, M. Gao, H. Pan, *J. Mater. Chem. A*, 2014, **2**, 3155.
- H. Cao, H. Wang, T. He, G. Wu, Z. Xiong, J. Qiu, P. Chen, *RSC Adv.*, 2014, **4**, 32555.
- L. Fernandez Albanesi, S. Garroni, P. Arneodo Larochette, P. Nolis, G. Mulas, S. Enzo, M. D. Baro, F. C. Gennari, *Int. J. Hydrogen Energy*, 2015, **40**, 13506.

## ARTICLE

JournalName

- 28 H.E. Kissinger, *Anal. Chem.*, 1957, **29**, 1702.
- 29 J. W. Makepeace, M. O. Jones, S. K. Callear, P. P. P. Edwards, W. D. I. F. David, *Phys. Chem. Chem. Phys.*, 2014, **16**, 4061.
- 30 G. Amica, P. Arneodo Larochette, F.C. Gennari, *Int. J. Hydrogen Energy*, 2015, **40**, 9335.



The  $\text{Li}_4(\text{NH}_2)_3\text{Cl}$ - $3\text{LiH}$  composite was synthesized by milling of  $\text{LiNH}_2$ - $\text{LiCl}$ - $3\text{LiH}$  and heating at  $200\text{ }^{\circ}\text{C}$  under  $6.0\text{ MPa}$  of hydrogen pressure.